Tumor Imaging in Patients with Advanced Tumors Using a New ^{99m}Tc-Radiolabeled Vitamin B12 Derivative

Bert-Ram Sah[*1], Roger Schibli[*2,3], Robert Waibel[2], Lotta von Boehmer[4], Peter Bläuenstein[2], Ebba Nexo[5], Anass Johayem[1], Eliane Fischer[2,3], Ennio Müller[1], Jan D. Soyka[1], Alexander K. Knuth[4], Stefan K. Haerle[6], Pius August Schubiger[2,3], Niklaus G. Schaefer[*1,4], and Irene A. Burger[*1]

[1]Division of Nuclear Medicine, Department Medical Radiology, University Hospital of Zurich, Zurich, Switzerland; [2]Center for Radiopharmaceutical Science, Paul Scherrer Institute, Villingen PSI, Switzerland; [3]Department of Chemistry and Applied Biosciences of the ETH Zurich, Zurich, Switzerland; [4]Division of Medical Oncology, Department of Internal Medicine, University Hospital of Zurich, Zurich, Switzerland; [5]Department of Clinical Biochemistry, Aarhus University Hospital, Aarhus C, Denmark; and [6]Department of Otolaryngology-Head and Neck Surgery, University Hospital of Zurich, Zurich, Switzerland

Targeting cancer cells with vitamin B12 (cobalamin) is hampered by unwanted physiologic tissue uptake mediated by transcobalamin. Adhering to good manufacturing practice, we have developed a new ^{99m}Tc-cobalamin derivative (^{99m}Tc(CO)$_3$-[(4-amido-butyl)-pyridin-2-yl-methyl-amino-acetato] cobalamin, ^{99m}Tc-PAMA-cobalamin). The derivative shows no binding to transcobalamin but is recognized by haptocorrin, a protein present in the circulation and notably expressed in many tumor cells. In this prospective study, we investigated cancer-specific uptake of ^{99m}Tc-PAMA-cobalamin in 10 patients with various metastatic tumors. **Methods:** Ten patients with biopsy-proven metastatic cancer were included. Dynamic imaging was started immediately after injection of 300–500 MBq of ^{99m}Tc-PAMA-cobalamin, and whole-body scintigrams were obtained at 10, 30, 60, 120, and 240 min and after 24 h. The relative tumor activity using SPECT/CT over the tumor region after 4 h was measured in comparison to disease-free lung parenchyma. Patients 3–10 received between 20 and 1,000 μg of cobalamin intravenously before injection of ^{99m}Tc-PAMA-cobalamin. The study population comprised 4 patients with adenocarcinomas of the lung, 3 with squamous cell carcinomas of the hypopharyngeal region, 1 with prostate adenocarcinoma, 1 with breast, and 1 with colon adenocarcinoma. **Results:** The median age of the study group was 61 ± 11 y. Six of 10 patients showed positive tumor uptake on ^{99m}Tc-PAMA-cobalamin whole-body scintigraphy. The scan was positive in 1 patient with colon adenocarcinoma, in 3 of 4 lung adenocarcinomas, in 1 of 3 hypopharyngeal squamous cell carcinomas, and in 1 breast adenocarcinoma. Renal uptake was between 1% and 3% for the left kidney. Predosing with cobalamin increased the tumor uptake and improved blood-pool clearance. The best image quality was achieved with a predose of 20–100 ug of cold cobalamin. The mean patient dose was 2.7 ± 0.9 mSv/patient. **Conclusion:** To our knowledge, we report for the first time on ^{99m}Tc-PAMA-cobalamin imaging in patients with metastatic cancer disease and show that tumor targeting is feasible.

Received Apr. 8, 2013; revision accepted Jul. 31, 2013.

For correspondence or reprints contact: Irene A. Burger, Division of Nuclear Medicine, Department of Radiology, University Hospital of Zurich, Raemistrasse 100, CH-8091 Zurich, Switzerland.

E-mail: Irene.burger@usz.ch

*Contributed equally to this work.

Published online Dec. 12, 2013.

Key Words: vitamin B12; cancer; transcobalamin receptors; haptocorrin; cobalamin

J Nucl Med 2014; 55:43–49
DOI: 10.2967/jnumed.113.122499

Selective targeting of cancer cells for imaging procedures or delivery of drugs or toxins is in focus for cancer therapy. The aim is to have a substance homing for cancer cells but nontoxic for other cells of the body. For this purpose, the use of vitamin B12 (cobalamin) delivered in a manner that favors uptake in cancer cells is advantageous. All living cells, including tumor cells, depend on cobalamin, a coenzyme for methionine synthase and methyl-malonyl-CoA mutase (*1*); furthermore, cobalamin has no known toxicity.

A complex transport process involving several soluble binding proteins and corresponding receptors ensure the transport of the vitamin from the intestine through the bloodstream to the target cell (*2,3*). Intrinsic factor, present only in the gastrointestinal tract, mediates the intestinal absorption of cobalamin. In the circulation, transcobalamin mediates the transport to the cells of the body. Two cellular receptors recognizing transcobalamin–cobalamin (holoTC) have been described. Megalin is a multifunctional receptor ensuring the uptake of holoTC filtered in the kidney, whereas the newly identified transcobalamin receptor CD320 is believed to promote the uptake of holoTC into all cells of the body, including cancer cells (*4*).

For many decades it has been recognized that certain cancer cells show an increased extracellular density of receptors able to promote the uptake of holoTC (*5–7*), and several studies have explored the use of cobalamin labeled with radioactive cobalt isotopes (^{57}Co, ^{58}Co, ^{60}Co) for cancer imaging (*8,9*). However, all studies showed a high uptake also in the liver, kidney, spleen, nasal cavity, salivary, and lachrymal glands. The same pattern was obtained when using cobalamin labeled with ^{111}In, ^{131}I, and ^{99m}Tc (*10–12*). Especially the problem of a high kidney uptake has to be solved to use a cobalamin uptake system for cancer imaging with the potential for radionuclide therapy.

In addition to transcobalamin and intrinsic factor, a third soluble cobalamin-binding protein, haptocorrin, participates in the transport of cobalamin. Haptocorrin carries the major part of circulating

cobalamin, but interestingly haptocorrin is not filtered in the kidney and no receptor recognizing haptocorrin has been identified in the kidney. The function of haptocorrin in the transport and use of cobalamin is unsettled (*2,13*). However, 2 unique features of haptocorrin are important for the concept of the present paper. Haptocorrin recognizes a broader spectrum of cobalamin derivatives than does intrinsic factor and transcobalamin, and haptocorrin may occur in an increased amount in patients with cancer (*14*). Using immunohistochemistry, we have shown an increased expression of haptocorrin in samples from patients with carcinomas of the lung, prostate, uterus, and ovary as well as squamous cell carcinomas of the skin, B-cell lymphomas, seminomas, anaplastic thyroid cancer, and bladder urothelial cancer (*15*). The results support and expand earlier studies on plasma levels of haptocorrin, where high levels have been encountered in patients with liver cancer and with chronic myeloid leukemia and also in patients displaying normal levels of transcobalamin (*16,17*).

We recently described a tailored vitamin B12 derivative, ^{99m}Tc-PAMA-cobalamin (^{99m}Tc(CO)$_3$-[(4-amido-butyl)-pyridin-2-yl-methyl-amino-acetato] cobalamin) able to bind to human haptocorrin but not to human transcobalamin (*15*), and using a mouse model we showed ^{99m}Tc-PAMA-cobalamin accumulation in haptocorrin-expressing tumors with limited uptake in liver and kidney (*14*). In the present study, we report the results of a pilot trial in patients with advanced cancer, exploring the role of ^{99m}Tc-PAMA-cobalamin in a clinical setting.

MATERIALS AND METHODS

Patients

Ten patients with biopsy-proven active malignant disease were prospectively selected in this study, approved by the local ethics committee and the institutional review board. All patients gave informed consent according to our local ethics committee. Each patient had an ^{18}F-FDG–positive PET/CT ($n = 9$) examination for visceral metastases or a positive skeletal scintigraphy ($n = 1$) result confirming osseous metastases within 7 d before ^{99m}Tc-PAMA-cobalamin scintigraphy. The patients were consecutively assigned to different presaturation protocols with cold cobalamin. No change in any medication between both examinations was allowed in the study protocol.

Preparation of ^{99m}Tc-PAMA-Cobalamin

^{99m}Tc-PAMA-cobalamin was prepared under the good manufacturing practice guidelines in compliance with the Swiss agency of therapeutic products (Swissmedic). Precursor $[^{99m}Tc(CO)_3(OH_2)_3]^+$ was prepared using Isolink kits (Covidien). Radiolabeling and quality control of ^{99m}Tc-PAMA-cobalamin was performed according to the following procedure: [Na][$^{99m}TcO_4$] was eluted from a ^{99}Mo/^{99m}Tc generator (CIS Bio Elumatic III) with a 0.9% saline solution. Precursor $[^{99m}Tc(CO)_3(OH_2)_3]^+$ was prepared using the Isolink technology (*18,19*). [Na][$^{99m}TcO_4$] (1.0–1.4 mL; 6–7 GBq) was added to an Isolink kit. The kit was heated for 20 min at 95°C. After that, it was cooled to room temperature and kept for 5 min before the 350 μL of neutralization solution (1 M HCl and 0.6 M phosphate buffer: 3:2) was added. 2-(*N*-morpholino) ethanesulfonic acid buffer (MES buffer; 100 μL; 1 M, pH 6.2) was added. The entire $[^{99m}Tc(CO)_3(OH_2)_3]^+$ solution was added to a lyophilized vial containing 35 ± 2 μg of EtO-PAMA-cobalamin (~20 nmol). The reaction was heated for 75 min at 70°C. The crude product was purified on a semipreparative high-performance liquid chromatography system (System Gold 126 Solvent Module, System Gold 168 UV/vis Detector, or α Spectra NaI Scintillation Detector 8ISW8/2 [Beckman Coulter]) using an XTerra RP8 column (5 μm, 3.0 × 150 mm; Waters) with a linear gradient of 14% solvent B to 70% (solvent A: 1 M acetate buffer/EtOH 10%; solvent B: ethanol 70%) in 0–20 min. From 20 to 30 min, the gradient remained constant before ramping back (from 30 to 35 min) to the initial ratio. The flow rate was 1 mL/min and ultraviolet detection at 240 nm. The product peak (maximum, 2 mL) was collected into a 25-mL vial containing 14 mL of phosphate-buffered saline (pH 7.4). After synthesis and purification, the solution was sterile-filtered.

Blood Sampling and Presaturation with Vitamin B12

Blood samples for routine measurement of cobalamin were collected before injection of ^{99m}Tc-PAMA-cobalamin. Blood samples for clearance determination were removed 30 min, 60 min, 90 min, and 4 h after injection of ^{99m}Tc-PAMA-cobalamin.

For the predosing of patients with cobalamin, Vitarubin Superconc (Streuli Pharma AG) was used. Patients receiving cobalamin had a single intravenous injection 1 h before the ^{99m}Tc-PAMA-cobalamin injection. Patients 1 and 2 received no cobalamin, patients 3–6 received 20 μg, patients 7 and 8 received 100 μg intravenously, and patients 9 and 10 received 1,000 μg intravenous cobalamin.

Data Acquisition

All imaging was performed at our institution on a dedicated SPECT/CT scanner (Infinia Hawkeye; GE Healthcare). Dynamic imaging was started immediately after injection of 300–500 MBq of ^{99m}Tc-PAMA-cobalamin with 5 s per frame and 120 frames (10 min). Thereafter, the first whole-body scintigram was started with a table speed of 30 s/cm. After 30 min, a second whole-body scintigram was obtained (table speed, 30 cm/s). This procedure was repeated after 60, 120, and 240 min (each with a table speed of 15 cm/s) and after 24 h (with a table speed of 10 cm/s). In addition, SPECT/CT was performed over the tumor region after 4 h, imaging with a step-and-shoot protocol of 30 s and a rotation angle of 3° for a total of 60 views per camera head. Images were reconstructed with iterative attenuation reconstruction on a 128 × 128 matrix. The CT (x-ray, 2.5 mA; 140 kV) had a slice thickness of 10 mm, with a scan time of approximately 10 min for a 40-cm field of view.

Data Analysis

Image analysis was performed by 2 nuclear medicine physicians in consensus. All imaging results using ^{99m}Tc-PAMA-cobalamin were compared with either ^{18}F-FDG PET/CT ($n = 9$) or bone scintigraphy ($n = 1$). Whole-body scintigrams at 10, 30, 60, 120, and 240 min and 24 h after administration were analyzed for relative tumor uptake. A region of interest over the whole liver, bladder (urinary), left kidney, lung, mediastinum, salivary glands, soft tissue, and tumor tissue was placed. The data were normalized using a whole-body region of interest at the given time point. Data were analyzed in the anterior and posterior views using the COMPARE ROI ANALYSIS algorithm in the Xeleris Workstation (GE Healthcare Biosciences).

The normalized activities were taken as relative activity after injection of 1 MBq of ^{99m}Tc. From these activities, the effective remaining activities were calculated with the half-life for ^{99m}Tc of 6 h. Between each time point, the effectively remaining activity (i.e., area under the curve) was estimated with the calculation over trapezoids (time difference multiplied by the height). Afterward, the area of the trapezoids for the different time points was summed. The results presented the input data of the software OLINDA, which calculates the specified organ doses in mSv/MBq. Finally, the doses were multiplied by the injected dose in megabecquerel per patient to get the effective dose per patient (mSv/patient).

^{99m}Tc-PAMA-cobalamin scintigrams were compared with recent ^{18}F-FDG PET/CT data ($n = 9$) or ^{99m}Tc-methylene diphosphonate bone scintigraphy ($n = 1$). The primary tumor was imaged with SPECT/CT after 4 h. Tumor-to-background activity ratios were estimated using normal lung tissue as background reference (kBq/cm^3) using dedicated software for SPECT image analysis (PMOD 3.3; PMOD Technologies).

TABLE 1
Patient Characteristics and Imaging Findings

Patient no.	Diagnosis	Lesion	Tumor location	Lesion size (cm)	^{18}F-FDG PET/CT	^{99m}Tc-PAMA-cobalamin scintigraphy findings	Reference
1	Hypopharyngeal cancer		Primary tumor in right hypopharynx			No focal uptake	
		Lesion 1	Right hypopharynx	1.3	TP	FN	Histopathology
2	Hypopharyngeal cancer		Primary tumor in left hypopharynx			No focal uptake	
		Lesion 1	Left hypopharynx	3.5	TP	FN	Histopathology
		Lesion 2	Lymph node cervical left	1.7	TP	FN	Histopathology
3	Colon cancer		Metastases in liver and muscles			Focal uptake in liver metastases	
		Lesion 1	Liver (multiple)	Up to 8.0	TP	TP	Histopathology
		Lesion 2	Left psoas muscle	2.7	TP	FN	^{18}F-FDG PET/CT
		Lesion 3	Left thoracic wall, 10/11 rip	1.8	TP	FN	^{18}F-FDG PET/CT
4	Non–small cell lung cancer		Primary tumor in left upper lobe of the lung			Intense uptake in primary tumor and metastasis	
		Lesion 1	Left upper lobe	3.8	TP	TP	Histopathology
		Lesion 2	Lymph node hilus left	3.2	TP	TP	^{18}F-FDG PET/CT
		Lesion 3	Lymph node mediastinal	1.0	TP	TP	^{18}F-FDG PET/CT
		Lesion 4	Bone metastases (several)	Up to 4.0	TP	FN	Histopathology
5	Hypopharyngeal cancer		Primary tumor in right hypopharynx			Intense uptake in primary and metastasis	
		Lesion 1	Right hypopharynx	4.8	TP	TP	Histopathology
		Lesion 2	Lymph node cervical right	3.1	TP	TP	Histopathology
		Lesion 3	Lymph node cervical left	1.9	TP	FN	Histopathology
6	Prostate cancer		Metastases in lymph node and bones		CT only	No focal uptake	
		Lesion 1	Lymph node retroperitoneal	1.9	TP	FN	CT
		Lesion 2	Bone metastases	up to 1.3	TP	FN	CT
7	Non–small cell lung cancer		Primary tumor in right upper lobe of the lung			Focal uptake in primary and metastasis	
		Lesion 1	Right upper lobe of the lung	2.1	TP	TP	Histopathology
		Lesion 2	Right lower lobe	0.9	TP	FN	^{18}F-FDG PET/CT
		Lesion 3	Left upper lobe	1.4	TP	TP	^{18}F-FDG PET/CT
		Lesion 4	Lymph node mediastinal	1.2	TP	TP	^{18}F-FDG PET/CT
8	Non–small cell lung cancer		Primary tumor in left upper lobe of the lung			Focal uptake in primary	
		Lesion 1	Left upper lobe	4.0	TP	TP	Histopathology
		Lesion 2	Left adrenal gland	4.1	TP	FN	Histopathology
9	Breast cancer		Lymph node metastases			Focal uptake in metastasis	
		Lesion 1	Lymph node cervical left	1.1	TP	FN	^{18}F-FDG PET/CT
		Lesion 2	Lymph node axillary right	0.9	TP	TP	^{18}F-FDG PET/CT
		Lesion 3	Lymph node axillary left	1.1	TP	FN	^{18}F-FDG PET/CT
		Lesion 4	Lymph node retroperitoneal	2.2	TP	FN	Histopathology
10	Non–small cell lung cancer		Primary tumor in left upper lobe of the lung			No focal uptake	
		Lesion 1	Left upper lobe	7.6	TP	FN	Histopathology
		Lesion 2	Pleura	2.5	TP	FN	^{18}F-FDG PET/CT
		Lesion 3	Sixth rib	1.7	TP	FN	^{18}F-FDG PET/CT
		Lesion 4	Left adrenal gland	1.7	TP	FN	^{18}F-FDG PET/CT

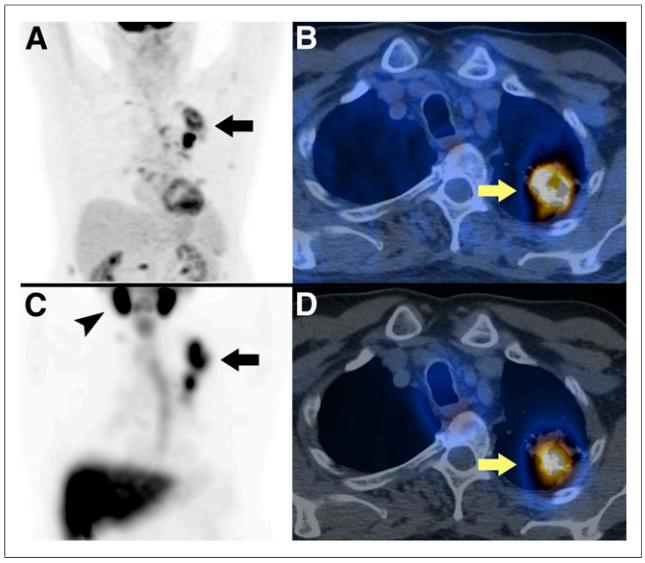

FIGURE 1. Results from a 61-y-old man with known bronchial carcinoma in left upper lobe. Shown are maximum-intensity-projection PET image (A) and axial fused PET/CT image (B) 42 min after injection of 348 MBq of ^{18}F-FDG and maximum-intensity-projection SPECT image (C) and axial fused SPECT/CT image (D) 4 h after injection of 587 MBq of ^{99m}Tc-PAMA-cobalamin. On maximum-intensity-projection image in A (^{18}F-FDG) and C (^{99m}Tc-PAMA-cobalamin), tumor is highly active on both images (arrows). In addition, C shows high tracer accumulation of ^{99m}Tc-PAMA-cobalamin in salivary glands (arrowhead) and liver. Mean relative tracer accumulation in different organs in relation to whole-body scan were liver, 28%; left kidney, 1%; lungs, 7%; and tumor, 3%.

^{99m}Tc-PAMA-cobalamin in blood samples was analyzed using a standard γ ray detector. Blood clearance ($t_{1/2}$) was calculated using injected dose per blood volume as injected reference concentration and decay-corrected blood-pool activities at 30, 60, 90, and 240 min. Exponential blood-pool elimination with 0 noise and no constraints was assumed, and blood-pool half-life was calculated with the least-square fitting method (MATLAB 7.9.0; The MathWorks).

RESULTS

Patient Demographics

Ten patients with various metastasized tumors were prospectively selected. The median age of the study group was 61 (range, 47–84 y) years. Four patients presented with adenocarcinomas of the lung, 3 with squamous cell carcinomas of the hypopharyngeal region, 1 with prostate adenocarcinoma, 1 with adenocarcinoma of the breast, and 1 with colon adenocarcinoma. Patient demographics are summarized in Table 1.

Qualitative Imaging Results of ^{99m}Tc-PAMA-Cobalamin Scintigraphy

Six of 10 patients with metastatic cancer had positive tumor delineation in ^{99m}Tc-PAMA-cobalamin scintigraphy. The ^{99m}Tc-PAMA-cobalamin scintigraphy result was positive in 1 patient with metastatic colon adenocarcinoma (patient 3), in 3 of 4 lung adenocarcinomas (patients 4, 7, and 8), in 1 of 3 hypopharyngeal squamous cell carcinomas (patient 5), and in 1 breast adenocarcinoma (patient 9). The ^{99m}Tc-PAMA-cobalamin scintigraphy result remained negative in 1 patient with prostate cancer with bone metastases (patient 6), 2 of the hypopharyngeal carcinomas (patients 1 and 2), and 1 lung cancer (patient 10). Lesion characteristics are summarized in Table 1.

Patients 1 and 2 suffered from hypopharyngeal squamous cell cancer. ^{99m}Tc-PAMA-cobalamin scintigraphy showed no focal uptake in the biopsy-proven and ^{18}F-FDG–active tumor tissue.

Patient 3 had a colon adenocarcinoma of the left colic flexure. At the time of the study scans, the primary tumor was resected. ^{18}F-FDG PET/CT showed metastases in the liver, in the left psoas muscle and between the 10th and 11th left rib. ^{99m}Tc-PAMA-cobalamin scintigraphy showed focal uptake in the liver metastases.

Patient 4 suffered from bronchial adenocarcinoma. ^{99m}Tc-PAMA-cobalamin scintigraphy showed high relative uptake of a factor of 45.0, compared with normal lung tissue in the primary tumor, and some focal uptake in mediastinal lymph nodes. ^{18}F-FDG PET/CT further delineated 2 local bone metastases not avid on ^{99m}Tc-PAMA-cobalamin scintigraphy (Fig. 1).

Patient 5 suffered from hypopharyngeal squamous cell cancer. ^{99m}Tc-PAMA-cobalamin scintigraphy showed intense uptake (tumor-to-background ratio, 55.6) in the right cervical lymph node and some lower focal uptake in the primary tumor in the central neck. ^{18}F-FDG PET/CT in this patient showed intense uptake in the primary tumor and in local cervical lymph node metastases bilaterally on level II/III and V (Fig. 2).

Patient 6 had a radical prostatectomy 2 y prior because of prostate adenocarcinoma. At the time of study, bone scintigraphy showed metastases in the left and right os ilium, whereas ^{99m}Tc-PAMA-cobalamin scintigraphy showed no relevant radiotracer uptake.

Patients 7 and 8 had bronchial adenocarcinomas. Both primary tumors were positive on ^{99m}Tc-PAMA-cobalamin scintigraphy, with a tumor-to-background ratio of 14.7 and 5.6, respectively. ^{18}F-FDG PET/CT showed additional metastases in both patients.

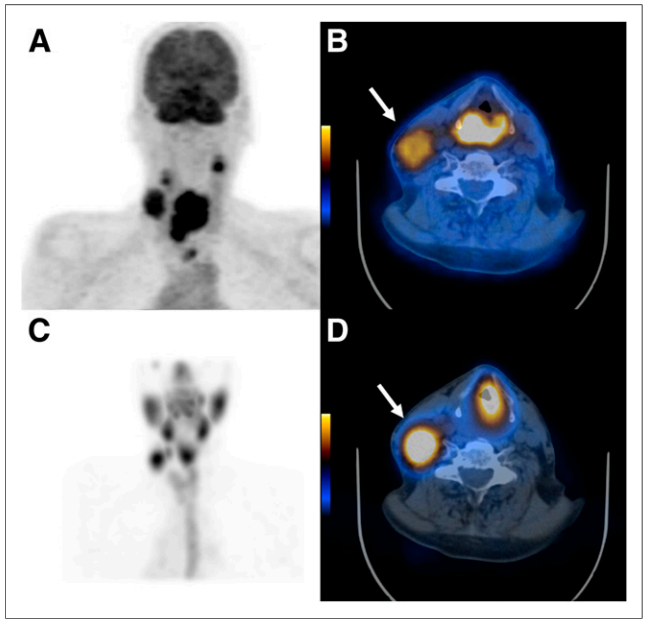

FIGURE 2. Results from a 67-y-old man with large hypopharyngeal carcinoma. Maximum-intensity-projection PET image (A) and axial fused PET/CT image (B) 45 min after injection of 355 MBq of ^{18}F-FDG and maximum-intensity-projection SPECT image (C) and axial fused SPECT/CT image (D) 4 h after injection of 503 MBq of ^{99m}Tc-PAMA-cobalamin. ^{99m}Tc-PAMA-cobalamin uptake was more intense in right cervical lymph node metastasis than ^{18}F-FDG uptake (arrow, B vs. D). Mean relative tracer accumulation in different organs in relation to whole-body scan were liver, 54%; left kidney, 2%; lungs, 4%; and tumor, 3%.

TABLE 2
Scan Information and Tumor Activities 4 Hours After Injection

Patient no.	^{99m}Tc-PAMA-cobalamin (MBq)	Dose (mSv/patient)	Cobalamin blood level (ng/L*)	Cobalamin predose (μg)	Average uptake after 4 h (kBq/cm^3)		
					Lung	Tumor	Relative
1	335	1.78	680	0	61	120	2.0
2	374	1.83	750	0	46	59	1.3
3	526	3.83	680	20	59	280	4.7†
4	575	2.45	280	20	29	1,304	45.0†
5	503	4.84	590	20	14	778	55.6†
6	495	3.36	740	20	9	1	0.1
7	383	2.85	440	100	5	74	14.7†
8	381	1.78	720	100	4	24	5.6†
9	456	2.21	230	1,000	8	25	3.3†
10	441	2.14	100	1,000	12	31	2.6

*For conversion to pmol/L, divide by 1,347.
†Tumors visualized on whole-body scintigraphy.

Patient 9 had an adenocarcinoma in the right breast, at study time resected. ^{18}F-FDG PET/CT showed metastases in the left cervical, bilateral axillary, and retroperitoneal lymph nodes. ^{99m}Tc-PAMA-cobalamin scans showed only a focal uptake in the right axilla.

Patient 10 had an ^{18}F-FDG–positive adenocarcinoma in the left upper lobe with pleural metastasis. The ^{99m}Tc-PAMA-cobalamin scintigraphy result was negative for all lesions.

Quantitative Organ and Tumor Uptake of ^{99m}Tc-PAMA-Cobalamin

An overview of injected ^{99m}Tc-PAMA-cobalamin doses and presaturation with cobalamin and the calculated tumor-to-background ratios and overall dose per patient are given in Table 2. The mean patient dose was 2.7 ± 0.9 mSv/patient (range, 1.8–4.8 mSv/patient).

In patients without cobalamin predose (patients 1 and 2), tumor tissue was not detectable on whole-body scintigrams (Fig. 3). The high values for lung (mean, 11.2%) and mediastinum (mean, 7.8%) reflect the high blood-pool activity over 24 h in both patients. The mean relative organ uptake for liver, salivary glands, and kidney was 14.6%, 3.3%, and 2.3%, respectively.

In patients who received cobalamin 60 min before injection of ^{99m}Tc-PAMA-cobalamin, the biodistribution pattern was significantly different. Tumor lesions were identified in 6 of 8 patients, with an average uptake of 4.6% of the injected dose to the tumors. The percentage activity in the tumors remained stable over 24 h, without significant washout (Fig. 3). The mean relative organ uptake after 20–100 μg of cobalamin for liver, salivary glands, and kidney was 20.9%, 3.6%, and 2.0%, respectively. Compared with the group without cobalamin, liver uptake in patients with cobalamin predose was considerably higher (Fig. 4). However, after predosing with 1,000 μg of cobalamin the mean organ activity for tumor tissue, liver, and salivary glands decreased to 0.5%, 4.3%, and 1.2%, respectively, whereas the renal activity remained around 2.0%. Relative tumor and organ uptake values 2 h after injection of ^{99m}Tc-PAMA-cobalamin are presented Table 3.

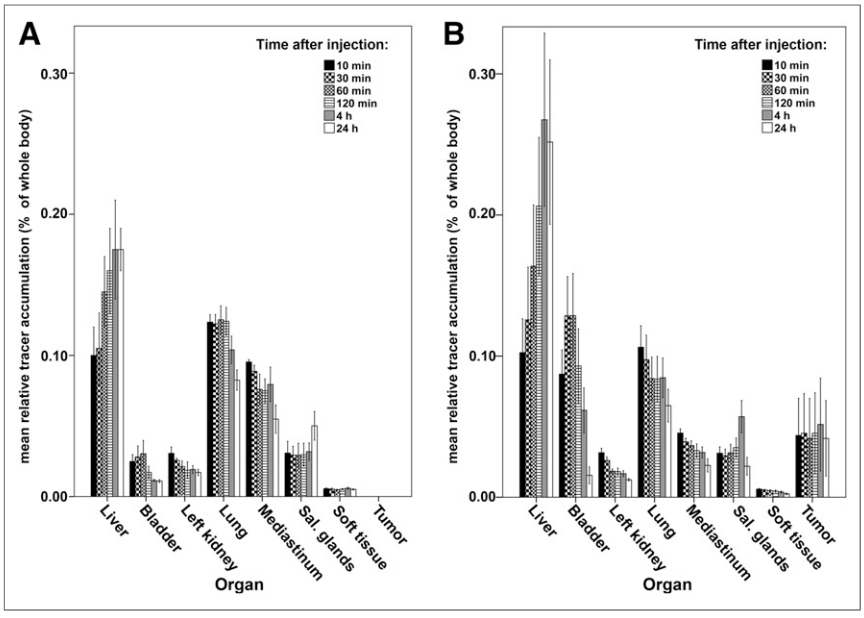

FIGURE 3. Mean relative tracer accumulation in different organs at different times after injection of tracer without prior injection of cobalamin (A) and with cobalamin predose (B). Sal. = salivary.

Blood Clearance of ^{99m}Tc-PAMA-Cobalamin

For patients without cobalamin predosing, radioactivity in the blood pool cleared with a half-life of about 10 h. In patients receiving cobalamin before ^{99m}Tc-PAMA-cobalamin, the half-life of the tracer in the blood was on average $t_{1/2}$ = 18 min (19 min for patients receiving 20–100 μg of cobalamin and 15.7 min for patients receiving 1,000 μg of cobalamin; Fig. 5).

DISCUSSION

This is the first, to our knowledge, clinical study confirming that a tailored

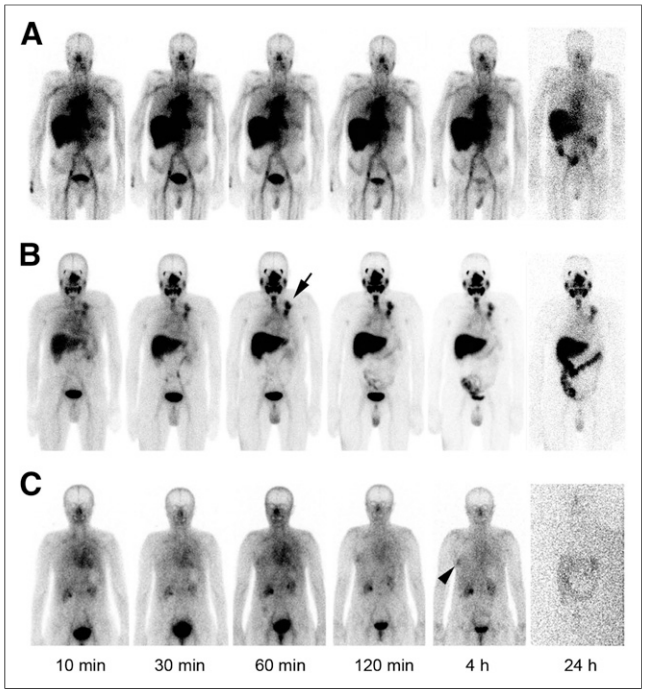

FIGURE 4. Partial-body scintigrams from head to pelvis were obtained for each patient after 10, 30, 60, 120, and 240 min and after 24 h. The three selected patients are illustrating influence of cobalamin predosing on distribution of ^{99m}Tc-PAMA-cobalamin. (A) Patient 2 without cobalamin predose has high blood-pool uptake over 24 h and no tracer accumulation in hypopharynx. (B) Patient 4 after 20-μg cobalamin predose has markedly reduced blood-pool activity and intense tracer uptake in bronchial carcinoma in left upper lobe (arrow) stable over 24 h. (C) Patient 9 after 1,000-μg cobalamin predose has reduced liver uptake and only faint ^{99m}Tc-PAMA-cobalamin activity in metastatic right axillary lymph node (arrowhead).

cobalamin derivative with abolished interaction to the transport protein transcobalamin but preserved affinity to haptocorrin can be used to visualize tumors in humans. It confirms results from an earlier preclinical study using a mouse model (*14*).

Several publications investigated cobalamin as a potential tumor tracer (*8–12*). First, the simple use of ^{57}Co-cyano-cobalamin confirmed an increased uptake in malignant cells (*8*), but the long half-life of ^{57}Co (272 d) restricted its use for clinical imaging. An ^{111}In-labeled diethylenetriaminepentaacetic acid (DTPA) adenosylcobalamin (^{111}In-DAC) with favorable dosimetry confirmed an increased tumor activity, however, with remaining high activities in the liver, spleen, kidney, and salivary glands. This has generally been attributed to the fact that the radiotracers bind to transcobalamin and hence are distributed to all cells carrying receptors for transcobalamin (*10*).

Similar to the results with ^{111}In-DAC, the new vitamin B12 derivative ^{99m}Tc-PAMA-cobalamin showed increased uptake in the salivary glands and liver. However, the abolished interaction to transcobalamin led to a reduction of renal organ dose, with an average uptake of 3.2% of the whole-body uptake in the left kidney after 10 min and a further decrease to 2% after 60 min and 1.7% after 24 h (Fig. 3).

Collins et al. described an increased tumor uptake with optimized visualization for patients with high blood-pool levels of cobalamin before injection of ^{111}In-DAC and suggested that the saturation of blood-pool transport protein could increase the tumor uptake (*20*). Our first 2 patients investigated without cobalamin predose confirmed a high blood-pool activity over 24 h, most likely due to tracer binding to apo-haptocorrin, which amounts to about 22 μg of blood per liter (0.3 nmol/L) in a normal healthy individual (*21*). Considering the small amount of PAMA-cobalamin injected per patient (~0.1–0.2 nmol), it is not surprising that most of the radiotracer bound to circulating haptocorrin. This would also coincide with the slow blood clearance, because haptocorrin-bound cobalamin is cleared from plasma with a $t_{1/2}$ of 9–12 d (*22*). The half-life of our tracer in the blood of patients without cobalamin was about 10 h, what corresponds closely to the effective half-life of a holo-haptocorrin–^{99m}Tc-PAMA-cobalamin complex. After cobalamin predosing, ^{99m}Tc-PAMA-cobalamin was excreted faster (average $t_{1/2}$ = 18 min) and had a lower blood-pool activity, presumably because the circulating haptocorrin was presaturated, therefore, relative liver and tumor uptake increased. However, after an injection of 1,000 μg of cobalamin the relative liver and tumor activities were significantly reduced, probably due to an oversaturation of haptocorrin in the blood and in organs and malignancies. In 5 of 6 patients receiving 20 or 100 μg of cobalamin, at least 1 lesion was visualized on the ^{99m}Tc-PAMA-cobalamin scintigram, with the highest tumor-to-background ratios after 20 μg of cobalamin. We therefore suggest that a range of 20–100 μg of cobalamin could yield the best image quality.

^{18}F-FDG PET/CT had the higher maximum standardized uptake value in the primary tumor, compared with the cervical lymph node (Fig. 2). Interestingly, ^{99m}Tc-PAMA-cobalamin scintigraphy showed the opposite: higher tracer uptake in the cervical lymph node metastasis than in the primary tumor. Histology work-up of this case showed a vital lymph node metastasis and large necrotic areas with inflammatory components within the primary tumor. However, ^{18}F-FDG PET/CT correctly staged this patient as cT4cN2cM0, because of contralateral lymph nodes, and therefore showed a relevant upstaging from N1 to N2c, compared with ^{99m}Tc-PAMA-cobalamin scintigraphy.

TABLE 3
Relative Uptake per Organ 2 Hours After Injection

Organ	Without cobalamin (n = 2) (%)	With cobalamin (%)			
		20 μg (n = 4)		100 μg (n = 2)	1,000 μg (n = 2)
		Mean	Range		
Tumor	0/0	7.7	1–19	0/1	0/0
Liver	13/19	32.5	25–39	17/8	3/5
Salivary glands	4/2	3	1–6	4/4	4/3
Lung	13/11	7.8	2–15	8/7	12/13
Mediastinum	8/7	3.8	2–6	3/3	2/4
Left kidney	2/1	1.25	1–2	2/2	3/2

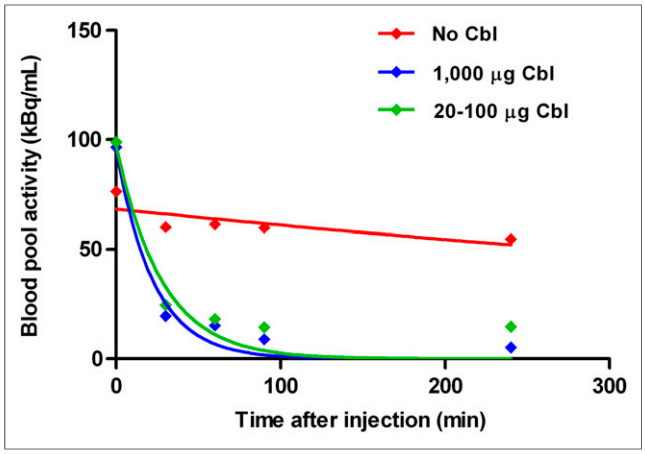

FIGURE 5. Blood clearance of ^{99m}Tc-PAMA-cobalamin: mean blood-pool activity 30, 60, 90, and 240 min after tracer injection with either no, 20- to 100-μg, or 1,000-μg cobalamin predose. Cbl = cobalamin.

In this proof-of-concept study, several different tumor types were analyzed. The resulting heterogeneous patient group is limiting the current study. However, previous immunohistochemistry studies for haptocorrin distribution on variable tumor cell lines revealed an overexpression in a large variety of different carcinomas (*15*). Our study confirmed an increased uptake of ^{99m}Tc-PAMA-cobalamin in bronchial adenocarcinoma, squamous cell cancer of the head and neck, breast cancer, and colon cancer.

Because of the small numbers and the heterogeneity of our study, we could not determine any disease-specific sensitivities or specificities for ^{99m}Tc-PAMA-cobalamin. Nevertheless, it is the first study in humans confirming that selective tumor imaging with ^{99m}Tc-PAMA-cobalamin is feasible in a large variety of different tumor histologies and shows a low renal uptake. Further studies with larger samples of patients with optimal predosing are needed.

CONCLUSION

In vivo tumor visualization is possible with the cobalamin derivative ^{99m}Tc-PAMA-cobalamin. After pretreatment with cobalamin to saturate circulating haptocorrin, the tracer accumulates in tumor tissue, liver, and salivary glands but not in the radiosensitive kidneys. Although the overall sensitivity was low, compared with ^{18}F-FDG PET/CT, the present results may pave the road for further development of radiotherapeutic drugs.

DISCLOSURE

The costs of publication of this article were defrayed in part by the payment of page charges. Therefore, and solely to indicate this fact, this article is hereby marked "advertisement" in accordance with 18 USC section 1734. No potential conflict of interest relevant to this article was reported.

ACKNOWLEDGMENTS

We thank the nuclear pharmacy, the technologists, and the administrative staff at the University Hospital of Zurich for their help in acquiring the data and freeing up resources. Specifically, we thank Verena Weichselbaumer and Miriam de Bloehme for the data acquisition. Furthermore, we thank Dr. Hansjoerg J. Treichler for initiating the project of tumor targeting with vitamin B12 derivatives and Christine DePasquale for valuable technical support.

REFERENCES

1. Waterhouse RN, Slifstein M, Dumont F, et al. In vivo evaluation of [^{11}C]N-(2-chloro-5-thiomethylphenyl)-N'-(3-methoxy-phenyl)-N'-methylguanidine ([^{11}C]GMOM) as a potential PET radiotracer for the PCP/NMDA receptor. *Nucl Med Biol.* 2004;31:939–948.
2. Nielsen MJ, Rasmussen MR, Andersen CB, Nexo E, Moestrup SK. Vitamin B12 transport from food to the body's cells: a sophisticated, multistep pathway. *Nat Rev Gastroenterol Hepatol.* 2012;9:345–354.
3. Fedosov SN. Physiological and molecular aspects of cobalamin transport. *Subcell Biochem.* 2012;56:347–367.
4. Quadros EV, Sequeira JM. Cellular uptake of cobalamin: transcobalamin and the TCblR/CD320 receptor. *Biochimie.* 2013;95:1008–1018.
5. Amagasaki T, Green R, Jacobsen DW. Expression of transcobalamin II receptors by human leukemia K562 and HL-60 cells. *Blood.* 1990;76:1380–1386.
6. Coudroy G, Gburek J, Kozyraki R, et al. Contribution of cubilin and amnionless to processing and membrane targeting of cubilin-amnionless complex. *J Am Soc Nephrol.* 2005;16:2330–2337.
7. Hall CA, Colligan PD, Begley JA. Cyclic activity of the receptors of cobalamin bound to transcobalamin II. *J Cell Physiol.* 1987;133:187–191.
8. Bose S, Komorowski R, Seetharam S, Gilfix B, Rosenblatt DS, Seetharam B. In vitro and in vivo inactivation of transcobalamin II receptor by its antiserum. *J Biol Chem.* 1996;271:4195–4200.
9. Collins DA, Hogenkamp HP. Transcobalamin II receptor imaging via radiolabeled diethylene-triaminepentaacetate cobalamin analogs. *J Nucl Med.* 1997;38:717–723.
10. Collins DA, Hogenkamp HP, Gebhard MW. Tumor imaging via indium 111-labeled DTPA-adenosylcobalamin. *Mayo Clin Proc.* 1999;74:687–691.
11. Mundwiler S, Waibel R, Spingler B, Kunze S, Alberto R. Picolylamine-methylphosphonic acid esters as tridentate ligands for the labeling of alcohols with the fac-$[M(CO)_3]^+$ core (M = ^{99m}Tc, Re): synthesis and biodistribution of model compounds and of a ^{99m}Tc-labeled cobinamide. *Nucl Med Biol.* 2005;32:473–484.
12. Ruiz-Sanchez P, Mundwiler S, Medina-Molner A, Spingler B, Alberto R. Iodination of cisplatin adduct of vitamin B-12. *J Organomet Chem.* 2007;692:1358–1362.
13. Morkbak AL, Poulsen SS, Nexo E. Haptocorrin in humans. *Clin Chem Lab Med.* 2007;45:1751–1759.
14. Arendt JF, Nexo E. Cobalamin related parameters and disease patterns in patients with increased serum cobalamin levels. *PLoS ONE.* 2012;7:e45979.
15. Waibel R, Treichler H, Schaefer NG, et al. New derivatives of vitamin B_{12} show preferential targeting of tumors. *Cancer Res.* 2008;68:2904–2911.
16. Carmel R. Extreme elevation of serum transcobalamin I in patients with metastatic cancer. *N Engl J Med.* 1975;292:282–284.
17. Carmel R, Eisenberg L. Serum vitamin B12 and transcobalamin abnormalities in patients with cancer. *Cancer.* 1977;40:1348–1353.
18. Alberto R, Ortner K, Wheatley N, Schibli R, Schubiger AP. Synthesis and properties of boranocarbonate: a convenient in situ CO source for the aqueous preparation of $[^{99m}Tc(OH_2)_3(CO)_3]^+$. *J Am Chem Soc.* 2001;123:3135–3136.
19. Alberto R, Schibli R, Egli A, et al. Metal carbonyl syntheses. XXII. Low-pressure carbonylation of $[MOCl_4]$- and $[MO_4]$-. The technetium(I) and rhenium(I) complexes $[NEt_4]_2[MCl_3(CO)_3]$. *J Organomet Chem.* 1995;492:217–224.
20. Collins DA, Hogenkamp HP, O'Connor MK, et al. Biodistribution of radiolabeled adenosylcobalamin in patients diagnosed with various malignancies. *Mayo Clin Proc.* 2000;75:568–580.
21. Sheppard K, Bradbury DA, Davies JM, Ryrie DR. Cobalamin and folate binding proteins in human tumour tissue. *J Clin Pathol.* 1984;37:1336–1338.
22. Burger RL, Schneider RJ, Mehlman CS, Allen RH. Human plasma R-type vitamin B_{12}-binding proteins. II. The role of transcobalamin I, transcobalamin III, and the normal granulocyte vitamin B12-binding protein in the plasma transport of vitamin B_{12}. *J Biol Chem.* 1975;250:7707–7713.

The Journal of NUCLEAR MEDICINE

Tumor Imaging in Patients with Advanced Tumors Using a New ^{99m}Tc-Radiolabeled Vitamin B12 Derivative

Bert-Ram Sah, Roger Schibli, Robert Waibel, Lotta von Boehmer, Peter Bläuenstein, Ebba Nexo, Anass Johayem, Eliane Fischer, Ennio Müller, Jan D. Soyka, Alexander K. Knuth, Stefan K. Haerle, Pius August Schubiger, Niklaus G. Schaefer and Irene A. Burger

J Nucl Med. 2014;55:43-49.
Published online: December 12, 2013.
Doi: 10.2967/jnumed.113.122499

The Journal of Nuclear Medicine is published monthly.
SNMMI | Society of Nuclear Medicine and Molecular Imaging
1850 Samuel Morse Drive, Reston, VA 20190.
(Print ISSN: 0161-5505, Online ISSN: 2159-662X)

SNMMI SOCIETY OF NUCLEAR MEDICINE AND MOLECULAR IMAGING